HHS Public Access

Author manuscript

*Nature*. Author manuscript; available in PMC 2017 January 14.

Published in final edited form as:

*Nature*. 2016 July 14; 535(7611): 303–307. doi:10.1038/nature18628.

# TTC39B Deficiency Stabilizes LXR Reducing both Atherosclerosis and Steatohepatitis

**Joanne Hsieh**[1,*], **Masahiro Koseki**[1,2,*,§], **Matthew M. Molusky**[1], **Emi Yakushiji**[1], **Ikuyo Ichi**[3], **Marit Westerterp**[1], **Jahangir Iqbal**[4], **Robin B. Chan**[5], **Sandra Abramowicz**[1], **Liana Tascau**[1], **Shunichi Takiguchi**[6], **Shizuya Yamashita**[2], **Carrie L. Welch**[1], **Gilbert Di Paolo**[5], **M. Mahmood Hussain**[4], **Jay H. Lefkowitch**[5], **Daniel J. Rader**[6], and **Alan R. Tall**[1,§]

[1]Division of Molecular Medicine, Department of Medicine, Columbia University, New York, NY 10032, USA

[2]Division of Cardiology, Department of Medicine, Osaka University Graduate School of Medicine, Suita, Osaka, Japan

[3]Faculty of Core Research, Ochanomizu University, Tokyo, Japan

[4]Department of Cell Biology, State University of New York Health Science Center at Brooklyn (SUNY Downstate Medical Center), Brooklyn, NY 11203, USA

[5]Department of Pathology and Cell Biology, Columbia University, New York, NY 10032 USA

[6]Departments of Genetics and Medicine, Perelman School of Medicine, University of Pennsylvania, Philadelphia PA 19104

## Summary

Cellular mechanisms that mediate steato-hepatitis, an increasingly prevalent condition in the Western world for which no therapies are available[1], are poorly understood. Despite the fact its synthetic agonists induce fatty liver, the Liver X receptor (LXR) transcription factor remains a target of interest because of its anti-atherogenic, cholesterol removal and anti-inflammatory activities. We discovered that tetratricopeptide repeat (TPR) domain protein 39B (*Ttc39b*, C9orf52) (*T39*), a high density lipoprotein (HDL) gene discovered in human genome wide association studies (GWAS)[2], promotes the ubiquitination and degradation of LXR. Chow-fed



[§]corresponding author. Address correspondence to: Alan R Tall: Division of Molecular Medicine, Department of Medicine, Columbia University 630 W 168th St, P&S 8-401, New York, NY 10032, USA. Phone: +1-212-305-5789; Fax: +1-201-305-5052, art1@cumc.columbia.edu Or Masahiro Koseki: Department of Cardiovascular Medicine, Osaka University Graduate School of Medicine, 2-2 Yamadaoka, Suita, Osaka 565-0871, Japan, Phone: +81-6-6879-3633; Fax: +81-6-6879-3634, koseki@cardiology.med.osaka-u.ac.jp.

[*]These authors contributed equally to the work

**Author Contributions:** J.H. and M.K. generated epitope-tagged constructs, bred mice, performed *in vivo* and cell culture experiments, collected data, designed the study, interpreted data, and wrote the paper; M.M.M. isolated hepatocytes and performed the ChIP and insulin sensitivity experiments; E.Y. and L.T. collected data; I.I. performed oxysterol and plant sterol measurements; M.W., S.A. and C.B.W. performed atherosclerotic lesion analysis; R.B.C and G.D. designed and performed lipidomics analyses; J.I. performed enterocyte *ex vivo* secretion studies; S.T. performed microarray analysis; J.H.L. performed histopathological analyses of liver sections; D.J.R., M.M.H. and S.Y. were involved in study design; A.R.T. designed the study, interpreted data and wrote the paper. All authors discussed the results and commented on the manuscript.

**Author Information:** No competing financial interests reported.

*T39*$^{-/-}$ mice displayed increased HDL cholesterol levels associated with increased enterocyte *ATP binding cassette transporter A1* (*Abca1*) expression and increased LXR protein without change in LXR mRNA. When challenged with a high fat/high cholesterol/bile salt (HF/HC/BS) diet, *T39*$^{-/-}$ mice or mice with hepatocyte-specific T39 deficiency showed increased hepatic LXR protein and target gene expression, and unexpectedly protection from steato-hepatitis and death. Western Type Diet (WTD)-fed *Low density lipoprotein receptor* (*Ldlr*)$^{-/-}$*T39*$^{-/-}$ mice showed decreased fatty liver, increased HDL, decreased LDL and reduced atherosclerosis. In addition to increasing hepatic *Abcg5/8* expression and limiting dietary cholesterol absorption, T39 deficiency inhibited hepatic sterol regulatory element binding protein 1 (SREBP-1, ADD1) processing. This was explained by an increase in microsomal phospholipids containing polyunsaturated fatty acids (PUFA), linked to an LXRα-dependent increase in expression of enzymes mediating PC biosynthesis and incorporation of PUFA into phospholipids. The preservation of endogenous LXR protein activates a beneficial profile of gene expression that promotes cholesterol removal and inhibits lipogenesis. T39 inhibition could be an effective strategy for reducing both steato-hepatitis and atherosclerosis.

## Main

Genome-wide association studies have uncovered a plethora of novel genetic loci associated with alterations in plasma lipoprotein levels[2,3] that have potential to provide insights into metabolic diseases such as atherosclerosis and fatty liver. Single nucleotide polymorphisms (SNPs) in intron 1 of *T39* were associated with reduced hepatic *T39* mRNA and increased HDL cholesterol levels[2]. However, the only clue to the cellular functions of T39 is that it contains three consecutive TPR motifs, suggesting it might function as a scaffolding protein mediating the association of HDL-regulating proteins. *T39* mRNA was highly expressed in liver and small intestine of chow-fed wild type (WT) mice and was reduced by >90% in *T39*$^{-/-}$ mice (ED Fig 1). HDL cholesterol levels were increased by ~22% in chow-fed *T39*$^{-/-}$ mice compared to WT (ED Fig 2a) while non-HDL cholesterol and triglyceride (TG) levels were unchanged (not shown). *T39*$^{-/-}$ mice challenged with 3 weeks of the HF/HC/BS diet had a 42% increase in HDL cholesterol levels (ED Fig 2a), a 45% increase in apolipoprotein A-1 (ApoA-1), the major protein component of HDL particles (ED Fig 2b), decreased very low density lipoprotein (VLDL)/chylomicron cholesterol levels (ED Fig 2c) and no difference in plasma TG levels (not shown). Gene expression microarrays of the liver of chow-fed *T39*$^{-/-}$ and WT mice showed no significant differences in genes potentially involved in the regulation of HDL, including *Apoa1*, *Scavenger receptor b1, Hepatic lipase* and *Abca1*,which accounts for over 90% of HDL formation[4] (not shown).

There is longstanding evidence that the intestine makes a substantial contribution to the production of HDL[5,6]. Small intestinal enterocytes from chow-fed *T39*$^{-/-}$ mice showed increased *Abca1* mRNA and protein (ED Fig 2d,e and Fig 1a). Protein levels of both isoforms of LXR, the major transcriptional activator of *Abca1*[7], were dramatically increased (Fig 1a and ED Fig 2e), while *Lxrα (Nr1h3, RLD1)* and *Lxrβ (Nr1h2, UR)* mRNA levels were unchanged (ED Fig 2d). We also observed induction of other intestinal LXR target genes including *Inducible degrader of LDLR* (*Idol*, *Mylip1*)[8] (ED Fig 2d). There was increased incorporation of [$^{3}$H]cholesterol into HDL-sized particles secreted from *T39*$^{-/-}$

enterocytes isolated from chow- (ED Fig 2f) and HF/HC/BS diet-fed mice (ED Fig 2g). On the chow diet, enterocyte-specific *T39* deletion in *Villin-Cre(+)T39$^{fl/fl}$* mice raised HDL-cholesterol, whereas hepatocyte-specific *T39* deletion in *Albumin-Cre(+)T39$^{fl/fl}$* mice had no effect, confirming the intestinal contribution to increased HDL (Fig 1b). T39 deficiency did not yield any difference in HDL-cholesterol on the *Lxrα$^{-/-}$* background (not shown). Together, these findings suggest that the major mechanism responsible for increased HDL levels in chow-fed *T39$^{-/-}$* mice is increased intestinal expression of *Abca1*, secondary to a post-transcriptional induction of LXR protein. Hepatocyte T39 deficiency did, however, increase HDL-cholesterol in mice fed the HF/HC/BS diet (Fig 1b), which was reversed by LXRα deficiency (not shown). This suggests that under inflammatory conditions induced by the HF/HC/BS diet, the liver also contributes to the HDL phenotype of *T39$^{-/-}$* mice, consistent with the previous report that *T39* knockdown mediated by adenovirus, which targets the liver and is inflammatory, raised HDL[2].

HF/HC/BS diets have been used as a model of steatohepatitis resembling human non-alcoholic steato-hepatitis (NASH)[9]. After 20 weeks of HF/HC/BS feeding we noticed a 4-fold reduction in mortality among *T39$^{-/-}$* mice ($p<0.05$) (Fig 1c), accompanied by decreased circulating alanine aminotransferase (ALT) levels (ED Fig 3a). Livers were smaller and less pale in the *T39$^{-/-}$* mice versus controls (ED Fig 3b), while there were no differences in body weight or gonadal fat pad weight (not shown). The livers of *T39$^{-/-}$* mice had less Oil Red O staining (Fig 1d) reflecting diminished hepatic TG (ED Fig 3c) and cholesteryl ester (ED Fig 3d) accumulation, fewer inflammatory foci consisting of neutrophils and lymphocytes (Fig 1e, ED Fig 3e), less hepatocellular ballooning degeneration (Fig 1e, ED Fig 3f), and less hepatocyte proliferation in *T39$^{-/-}$* mice (ED Fig 3g). Mortality studies in tissue-specific T39 knockout mice revealed that protection was entirely due to hepatic T39 deficiency (Fig 1f). The livers of *Albumin-Cre(+)T39$^{fl/fl}$* mice had less perisinusoidal and periportal fibrosis compared to the *T39$^{fl/fl}$* and *Villin-Cre(+)T39$^{fl/fl}$* mice (Fig 1g and ED Fig 4a,b), reduced inflammation (ED Fig 4a,c) and less hepatocellular ballooning (ED Fig 4a,d). In the livers of *T39$^{-/-}$* mice fed HC/HF/BS for 6 weeks, many LXR targets were upregulated, including *Abcg5/8, Stearoyl coenzyme A desaturase 1 (Scd1), Elongation of very long chain fatty acids protein 5* (*Elovl5*), *Insulin induced gene 2a* (*Insig2a*) and *Lysophatidylcholine acyltransferase 3* (*Lpcat3*, *Mboat5*)[10], and these increases were reversed in *Lxrα$^{-/-}$T39$^{-/-}$* mice (Fig 2a). However, expression of lipogenic genes *Srebf1* and *Fatty acid synthase* (*Fasn*) was unchanged (Fig 2a). There was no difference in LXRα protein expression between WT and *T39$^{-/-}$* mice fed chow (Fig 2b). However, whereas feeding a HF/HC/BS diet reduced hepatic LXRα protein levels in WT mice, LXR protein levels in *T39$^{-/-}$* livers were largely preserved (Fig 2b,c), without any difference in *Lxrα* mRNA level (ED Fig 5a). Similar mRNA levels of *Sulfotransferase 2b1* (*Sult2b1*) and *Abcc1* were found in livers from both genotypes, suggesting that decreased LXR ligand sulfation and export[11] did not account for increased LXR target gene expression in *T39$^{-/-}$* mice (not shown). Also, hepatic levels of natural LXR ligands, including 24*S*-, 25-, 27-hydroxycholesterol and desmosterol, were decreased in whole body (ED Fig 5b) and unchanged in hepatocyte-specific T39 knockout mice (ED Fig 5c). Thus increased hepatic expression of LXR target genes in *T39$^{-/-}$* mice (Fig 2a) was primarily due to a post-transcriptional increase in LXR protein. Differences in serum ALT levels were abrogated in mice lacking LXRα (Fig 2d), indicating that LXR

activation is critical to the hepatoprotective effects of T39 deficiency. *T39*$^{-/-}$ mice had decreased dietary cholesterol absorption (Fig 2e), consistent with observations that hepatic and intestinal LXRα activation have been shown to decrease dietary cholesterol absorption[12,13]. There was also delayed postprandial plasma TG accumulation in *T39*$^{-/-}$ mice (Fig 2f). Reduced cholesterol absorption was LXRα-dependent (ED Fig 5d), and associated with reduced accumulation of exogenously-derived hepatotoxic oxysterols such as 7β-hydroxycholesterol, and 7-ketocholesterol (ED Fig 5b). The decrease in cholesterol absorption was not associated with a change in intestinal *Niemann Pick C1 Like 1* (*Npc1l1*) expression (ED Fig 5e) and persisted in the presence of the NPC1L1 inhibitor ezetimibe (Fig 2e), suggesting that these changes are attributable to upregulation of the sterol exporters ABCG5/8 (Fig 2a), which reduces fractional cholesterol absorption[14]. Consistent with ABCG5/8 induction[14], hepatic concentrations of the plant sterol campesterol were lower in *T39*$^{-/-}$ mice (ED Fig 5f), and there was enhanced reverse cholesterol transport (ED Fig 5g). While the decrease in sterol absorption could contribute to liver protection, both *Alb-Cre(+)T39*$^{fl/fl}$ and *Vil-Cre(+)T39*$^{fl/fl}$ mice exhibited significantly decreased cholesterol absorption (ED Fig 5h), whereas only the liver knockout was protective (Fig 1f), suggesting there must be another mechanism contributing to the hepatoprotective effect of T39 deficiency.

LXR activation by synthetic agonists has traditionally been associated with hypertriglyceridemia and hepatic steatosis, due to induction of SREBP-1c, the transcription factor that controls lipogenic gene expression[15]. However, in enterocytes and livers of *T39*$^{-/-}$ mice, *Srebf1* mRNA and precursor protein were not induced (ED Fig 2d, Fig 2a and Fig 2b). Notably, there was a dramatic inhibition of SREBP-1 processing to the smaller, transcriptionally-active form in the livers of *T39*$^{-/-}$ mice fed the HF/HC/BS diet (Fig 2b). The processing of SREBP-2, which is the transcription factor that regulates cholesterogenesis, was not affected (ED Fig 6a). The decrease in the mature form of SREBP-1 associated with T39 deficiency was LXRα-dependent (ED Fig 6b). *T39*$^{-/-}$ mice fed the WTD also had reduced hepatic TG (ED Fig 6c) and cholesterol (ED Fig 6d) accumulation, and inhibition of SREBP-1 processing (ED Fig 6e). Potentially contributing to decreased SREBP-1 processing, in the fasting state, there was marked LXRα-dependent induction of *Insig2a* (Fig 2a), the polytopic protein that retains SCAP and therefore SREBP in the endoplasmic reticulum, thereby preventing SREBP proteolytic cleavage. However, *Insig2a* is only induced by LXR in the absence of insulin[16], while SREBP-1 activation is prominent in the postprandial state when insulin levels are elevated, suggesting there must be a separate more physiologically relevant mechanism regulating SREBP-1 maturation.

In a fasting-refeeding experiment, WTD-fed *T39*$^{-/-}$ mice displayed significantly decreased hepatic TG synthesis *in vivo* (Fig 3a). The reduction in TG synthesis was accompanied by decreased expression of many lipogenic genes, including *Scd1, Elovl5, Acetyl-CoA carboxylase α (Accα)*, *Glycerol-3-phosphate acyltransferase (Gpat1, Gpam)*, and *Glucose-6-phosphate dehydrogenase* (*G6pd*), as well as *Patatin-like phospholipase domain-containing protein 3* (*Pnpla3, Adiponutrin*), which is an SREBP-1 target implicated in human hepatic steatosis[17,18] (Fig 3b). *AlbuminCre(+)T39*$^{fl/fl}$ mice also had significant reductions in postprandial hepatic lipogenic gene expression (ED Fig 6f). Since exogenous free fatty acids are the major source of hepatic TG in high fat diet fed mice[19], the decrease in

[$^3$H]-labelled TG observed in Figure 3D is likely due to lower rates of esterification of exogenous FA, possibly due to decreased hepatic *Gpat1* expression (Fig 3b) and delayed dietary TG absorption (Fig 2f). Hepatic insulin sensitivity did not differ between *T39*$^{-/-}$ and WT mice, as glucose tolerance (ED Fig 6g), hepatic gluconeogenesis (ED Fig 6h) and insulin-induced Akt phosphorylation were similar in WT and *T39*$^{-/-}$ mice (ED Fig 6i).

Microsomal lipid composition changes could have a sustained effect on SREBP-1 processing in the fed state. Among the most significant changes in the membrane lipids was a 30% increase in PC content in *T39*$^{-/-}$ mice, with no differences in phosphatidylethanolamine (PE) and phosphatidylserine (PS) (not shown). The increased in PC may be attributable to LXRα-dependent upregulation of the Kennedy Pathway enzymes, *Phosphate Cytidyltransferase 1a* (*Pcyt1a*) and *Choline/ethanolamine phosphotransferase 1* (*Cept1*) (Fig 2a). Enzymes involved in an alternate methylation-dependent PC synthesis pathway were not changed (Fig 2a). PC synthesis is an important regulator of SREBP-1 proteolytic maturation in the liver [20]. In the ER, LPCAT3-mediated phospholipid remodelling preferentially acylates the *sn*-2 position of lysophosphatidylcholine, lysophosphatidylethanolamine, and lysophosphatidylserine with PUFA[21]. There was a decreased ratio of lysophosphatidylcholine to PC (Fig 3c), and PC, PE and phosphatidylserine PS species all had significantly increased PUFA content (Fig 3d,e,f), consistent with *Lpcat3* upregulation[22]. PUFAs have been demonstrated to inhibit the transcription and processing of SREBP-1c[23]. Also, LPCAT3 activity ameliorates ER stress[10], which affects SREBP-1 processing[24]. Together these data suggest that an LXRα-dependent increase in PC synthesis and incorporation of PUFA into multiple phospholipid species in *T39*$^{-/-}$ mice may be a major factor inhibiting the development of NAFLD.

*T39*$^{-/-}$ mice were crossed into the *Ldlr*$^{-/-}$ background and fed a WTD to determine if the anti-atherogenic effects of LXR activation were maintained. Male *Ldlr*$^{-/-}$*T39*$^{-/-}$ mice had significantly lower total cholesterol and higher HDL-cholesterol (ED Fig 7a). Both male and female *Ldlr*$^{-/-}$*T39*$^{-/-}$ mice showed a reduction in LDL cholesterol (ED Fig 7a,b), but plasma TG levels were not different (not shown). Atherosclerotic lesion area evaluated by *en face* oil red O staining of the aorta was significantly reduced in *Ldlr*$^{-/-}$*T39*$^{-/-}$ mice compared to *Ldlr*$^{-/-}$ controls (Fig 3g). Although there was no difference in overall lesion area in the proximal aorta (ED Fig 7c), atherosclerosis was less advanced as judged by reduced lesion complexity in *Ldlr*$^{-/-}$*T39*$^{-/-}$ mice (ED Fig 7d). Thus, T39 deficiency confers protection from atherosclerosis and fatty liver following challenge with the WTD.

In contrast to the liver, in cultured primary hepatocytes from chow fed *T39*$^{-/-}$ mice, the mRNA levels of LXR target genes (*Srebf1, Scd1, Abcg5* and *Abcg8*) were increased, while expression of *Lxrα* and *Lxrβ* were unchanged (Fig 4a). LXRα protein was increased in the cytosol and nucleus of *T39*$^{-/-}$ hepatocytes (ED Fig 8a). We used the obligate heterodimer partner of LXR, retinoid X receptor (RXR) as a surrogate for the presence of LXR over LXR response elements (LXREs). There appeared to be increased occupancy by LXR/RXR over LXREs of several LXR targets in both the basal state and following GW3965 treatment in *T39*$^{-/-}$ vs WT hepatocytes (Fig 8b). In co-overexpression studies, LXRα coimmunoprecipiated with T39 regardless of the epitope tag size (Fig 4b), indicating that LXRα and T39 coexist in the same protein complex. We discovered that endogenous LXR

could be isolated using immobilized GW3965 (ED Fig 8c). In mice treated with a proteasome inhibitor, there was significantly less polyubiquitinated LXRα relative to unmodified LXRα in T39-deficient livers (Fig 4c). There was a significantly slower rate of LXRα turnover in *T39*$^{-/-}$ versus WT hepatocytes (Fig 4d). While the proteasome inhibitor bortezomib increased LXR in WT hepatocytes, it had no effect in *T39*$^{-/-}$ hepatocytes (Fig 4d). These data suggest that T39 facilitates LXRα polyubiquitination and turnover, and that in *T39*$^{-/-}$ cells, LXRα is protected from proteasomal degradation. We found a significant inverse correlation between published data on LXRα binding strength to active regulatory elements in the liver[25] and the magnitude of target gene induction in T39 deficiency relative to WT (ED Fig 8d), suggesting that the impact of increased LXR protein levels is larger for genes containing lower affinity LXR binding sites, such as *Insig2a* and *Lpcat3*, and minimally affects genes containing high affinity LXR binding sites, including *Srebf1* and *Fasn*. Hepatic LXR overexpression has been reported to upregulate cholesterol removal genes such as *Abcg5/8*[26], which is consistent with our findings. However, there were minimal effects on SREBP-1 target genes[26], suggesting that decreased LXR ubiquitination may also contribute to the decreased lipogenesis in *T39*$^{-/-}$ mice.

The deficiency of T39 demonstrates that as opposed to the effects of potent synthetic ligands, decreasing the ubiquitination and increasing the abundance of endogenous LXR protein can activate anti-atherogenic cholesterol removal while inhibiting the lipogenesis that leads to steatosis (ED Fig 9). By ameliorating CVD and NAFLD, T39 inhibition could offer a new therapeutic approach to tackle two globally prevalent chronic diseases.

## Extended Materials

### Methods

**Mice and Diet—**Both male and female 10-20 week old littermate mice were used in this study, and mice were allocated to experiments to match age and sex. *T39*$^{-/-}$ mice on the C57Bl/6N background were obtained from the Wellcome Trust Sanger Institute (Hinxton, UK). *Ldlr*$^{-/-}$*T39*$^{-/-}$ mice were generated by crossing these mice with *Ldlr*$^{-/-}$ mice from Jackson Laboratory (Bar Harbor, ME). *Lxrα*$^{-/-}$*T39*$^{-/-}$ mice were generated by crossing *T39*$^{-/-}$ mice with *Lxrα*$^{-/-}$ mice from Jackson Laboratory. For all backgrounds, *T39*$^{+/+}$ and *T39*$^{-/-}$ mice were generated by breeding *T39*$^{+/-}$ mice. Tissue-specific T39 knockout mice were generated by crossing *T39*$^{fl/fl}$ mice from Merck/TaconicArtemis (Germany) with *Villin-Cre* and *Albumin-Cre* mice obtained from the Jackson Laboratory. At 8 weeks of age, mice were started on either non-irradiated HF/HC/BS diet (7.5% cocoa butter, 1.25% cholesterol, 0.5% sodium cholate, no. 88051) or irradiated WTD (21% milk fat, 0.15% cholesterol, no. 88137) (Harlan Teklad). Mice were housed in a specific pathogen-free facility on a 12h:12h light:dark cycle. Compatible mice of mixed genotypes were housed in groups of 5. Each mouse was assigned a unique identification number that did not indicate genotype, and experiments and measurements were conducted in a blinded manner until data analysis. Animal numbers were selected based on power calculations of 0.8 using variances from previous studies and availability of genotypes that arose from heterozygote breedings. Protocols were approved by the Institutional Animal Care and Use Committee of Columbia University.

**Lipoprotein Analysis—**For chow and HF/HC/BS diet-fed samples, HDL-cholesterol was determined in the supernatant of phosphtungstate/$Mg^{2+}$-precipitated serum using an enzymatic-based colourimetric assay (Wako). Enzymatic-based colourimetric assays were also used to determine total serum cholesterol (Wako) and TG (Infinity Triglycerides, Thermo Scientific). For WTD-fed *Ldlr*$^{-/-}$ mice, lipoproteins were separated by KBr density ultracentrifugation and then assayed using the above kits.

**Enterocyte harvest, protein extraction, and Western blotting—**Enterocytes were collected from the jejunum using Cell Recovery Solution (BD) in a method adapted from Perreault *et al*[27]. Enterocytes and liver samples were homogenized in 1% Triton X-100, 0.5% sodium deoxycholate, 2 mM EDTA, and 1 mM EGTA in phosphate buffered saline, pH 7.4. Cytoplasmic and nuclear fractions were extracted from hepatocytes using the CelLytic NuCLEAR Extraction kit (Sigma-Aldrich) according to manufacturer's instructions. Proteins were resolved by SDS-PAGE and transferred to a polyvinylidene fluoride membrane for Western blotting. Western blotting antibodies were rabbit anti-LXRα/β (H-144, Santa Cruz Biotechnology), mouse anti-LXRα (PPZ0412, Abcam), rabbit anti-ABCA1 (NB400-105, Novus Biologicals), mouse anti-SREBP1 (clone 2A4, Thermo Scientific), rabbit anti-HSP90 (C45G5, Cell Signaling), goat anti-histone H3 (ab12079, Abcam), mouse anti-polyubiquitinated proteins (clone FK2, Millipore), and rabbit anti-SREBP-2 (14508-1-AP, Proteintech Group). An affinity-purified antibody against mouse and human T39 was generated by immunizing rabbits for 118 days against a conjugated amino acid sequence of T39, $NH_2$- CKESKWSKATYVFLKAAILS-COOH (Covance). The integrated density value of immunoblot signals was quantified by AlphaEaseFC software (Alpha Innotech).

**Secretion of [$^3$H]cholesterol by primary enterocytes—**For characterization of secreted lipoproteins, enterocytes were isolated from overnight fasted mice, and radiolabeled for 1 h with 0.5 μCi/ml of [$^3$H]cholesterol, washed, and incubated with fresh media containing lipid/bile salt micelles consisting of 1.4 mM oleic acid, 0.14 mM sodium cholate, 0.15 mM sodium deoxycholate, 0.17 mM phosphatidylcholine, and 0.19 mM mono-oleoylglycerol[28,29]. After 2 h, enterocytes were centrifuged and supernatants were collected. Media were subjected to density gradient ultracentrifugation to determine radiolabeled cholesterol distribution among lipoprotein classes[29].

**NASH grading—**Frozen sections of liver were stained with hematoxylin and eosin. Livers from mice fed HF/HC/BS diet were assessed by a blinded observer at 200× magnification according to the staging outlined by Kleiner and Brunt[30]. The lobular inflammation grade was assigned a score from 0 to 3 as follows: no foci = 0, less than 2 foci per field = 1, 2-4 foci per field = 2, more than 4 foci per field = 3. Liver cell injury was assigned a score from 0 to 2 as follows: no ballooned cells = 0, a few ballooned cells = 1, many ballooned cells = 2, majority of hepatocytes are ballooned = 3. The fibrosis grade was assigned a score from 0 to 3 as follows: no fibrosis = 0, scattered centrilobular and perisinusoidal areas of fibrosis = 1, many regions of fibrosis and true bridging = 2, extensive fibrosis and bridging, with/without cirrhosis = 3.

**Dietary cholesterol absorption—**Mice were fasted for 14 h and then given an intraperitoneal injection of Poloxamer-407 (1000 mg/kg, Sigma-Aldrich) to inhibit peripheral TG-rich lipoprotein catabolism. The mice were administered 10 μCi [$^3$H]cholesterol (PerkinElmer) in 135 μL olive oil containing 0.1 mg cold cholesterol, and blood was sampled from the tail vein every 4 hours. To inhibit NPC1L1, mice were gavaged with ezetimibe (10 mg kg$^{-1}$, Selleckchem) once daily for 3 days prior to the experiment.

**Sterol analysis and GC-MS analysis—**Oxysterols were measured as previously described[31]. 19-hydroxycholesterol (Steraloids) was added to samples as an internal standard. Lipids were extracted from plasma (50 μl) or livers (50 mg wet weight) with chloroform/methanol/water (1:2:0.8, v/v) containing butylated hydroxytoluene according to the Bligh and Dyer method[32]. Then the lipids were saponified at room temperature overnight in the dark. Unsaponified lipid was applied to a Sep-Pak Vac silica cartridge (Waters) to separate oxysterols and sterols[33]. Trimethylsilyl derivatives of the sterols were quantified by gas chromatography-mass spectrometry using a GC/MS QP2010 (Shimadzu) equipped with a SPB-1 fused silica capillary columm (60 m × 0.25 mm × 0.25 μm; Spelco). In the oven temperature program, the temperature was initiated at 180 °C for 1 min and then raised to 250°C at 20°C/min and to 290°C at 5 °C/min then held for 45 min. The injection temperature was set at 300°C, the interface at 300°C, and the ion source adjusted to 200°C.

***In* vivo determination of *de novo* lipogenesis—**WTD-fed mice were fasted overnight and then refed for 4 h. Mice were given an intraperitoneal injection of 1.5 mCi [$^3$H]water, and the liver was harvested 2 h later. Hepatic lipids were extracted by the Folch method and resolved by thin layer chromatography. The lipid spots visualized by iodine were scraped and $^3$H incorporation was determined by liquid scintillation counting. Biosynthetic rate was calculated essentially as described previously by Spady and Dietschy[34].

**Lipidomics analysis—**Microsomes were isolated from livers from HF/HC/BS diet-fed mice. Briefly, livers were homogenized with a Dounce homogenizer in a KCl-sucrose buffer (0.05 M $KH_2PO_4$, 0.25 M sucrose, 0.154 M KCl, pH 7.5) supplemented with protease inhibitors. Cellular debris, mitochondria, nuclei and plasma membrane were removed with a 10,000 ×g centrifugation, and microsomes were pelleted with a 100,000 ×g ultracentrifugation. Lipids were extracted by the Folch method in chloroform:methanol supplemented with butylated hydroxytoluene. Lipid extracts of purified microsome were spiked with a cocktail of internal standards, and analyzed using a 6490 Triple Quadrupole LC/MS system (Agilent Technologies). Glycerophospholipids and sphingolipids were separated with normal-phase HPLC as described before[35], with a few modifications. A Zorbax Rx-Sil column (inner diameter 2.1 × 100 mm, Agilent) was used under the following conditions: mobile phase A (chloroform:methanol:1 M ammonium hydroxide, 89.9:10:0.1, v/v) and mobile phase B (chloroform:methanol:water:ammonium hydroxide, 55:39.9:5:0.1, v/v); 95% A for 2 min, linear gradient to 30% A over 18 min and held for 3 min, and linear gradient to 95% A over 2 min and held for 6 min. Quantification of lipid species was accomplished using multiple reaction monitoring (MRM) transitions and instrument settings that were determined in earlier studies[35] in conjunction with referencing of known amounts

of internal standards: PA 14:0/14:0, PC 14:0/14:0, PE 14:0/14:0, PI 12:0/13:0, PS 14:0/14:0, SM d18:1/12:0, (Avanti Polar Lipids).

**Atherosclerosis Study—***Ldlr*$^{-/-}$ and *Ldlr*$^{-/-}$,*T39*$^{-/-}$ mice were fed WTD for 20 weeks. Mice were sacrificed in accordance to the American Veterinary Association Panel. Hearts and aortas were perfused with phosphate buffered saline, isolated and fixed in neutral phosphate-buffered formalin. The aortic arch and the descending aorta were stained with Oil Red O. Aortas were pinned on silicon dishes and Oil Red O positive areas were quantified using Image J software and expressed as the percentage of the total aorta area. Hearts were dehydrated, embedded in paraffin, and the aortic root area was cross-sectioned in 5 μm sections. The sections were stained with hematoxylin and eosin and the average of 6 evenly distributed sections for each animal was used to determine lesion size and complexity. Lesion size was quantified by morphometric analysis using Image-Pro Plus software (Media Cybernetics). The typing of lesions is done according to the typing for humans proposed by the American Heart Association[36] and adapted to categorize murine lesions[37]. In this study, we discerned sections showing macrophage foam cell rich lesions (type I-II), complex lesions with fibrous caps (type III), and advanced lesions with foam cells in the media and presence of fibrosis, cholesterol clefts, mineralization and/or necrosis (type IV-V).

**Plasmids—**Human *T39* was cloned from HepG2 cDNA into pCMV6-AN-GFP, pCMV6-Entry, and pCMV6-AN-Myc-DDK vectors (Origene) linearized by SgfI and MluI digestion using the In-Fusion PCR cloning kit (Clontech). Using the same approach, murine *Nr1h3* cDNA in the pCMV-SPORT6 vector (DF/HCC DNA Resource Core, Harvard University) was subcloned into the pCMV6-Entry and pCMV6-AN-Myc-DDK vectors.

**Primary hepatocyte culture and transfection—**Hepatocytes were isolated from 6-12 week old littermate mice using the two-step perfusion method and seeded onto collagen I-coated dishes (BD Biocoat) at a density of $2.5 \times 10^4$ cells/cm$^2$ in DMEM (Cellgro) containing 10% fetal bovine serum (Gibco) and 1% penicillin/streptomycin (Gibco). Cells were crosslinked and harvested for ChIP analysis 2 h following hepatocyte isolation. Hepatocytes were transfected the following day using JetPEI-Gal (Polyplus) according to the manufacturer's instructions and experiments were performed 3 days post-transfection.

**Cell culture and transfection—**HEK293T cells (ATCC) were propagated in DMEM containing 10% fetal bovine serum and 1% penicillin/streptomycin. Cells were transfected with Lipofectamine 2000 (Invitrogen) according to manufacturer's instructions. Cells were not tested for mycoplasma contamination after receipt from the ATCC.

**Chromatin immunoprecipitation—**Mouse hepatocytes were harvested and cultured as described above. At the time of plating hepatocytes were treated with either DMSO or 2 μM GW3965. Two hours post-treatment hepatocytes were cross-linked in 1% formaldehyde, at room temperature, for 10 or 20 minutes (depending on IP). The cross-linking reaction was quenched using 0.125M glycine (10 mins at room temperature). Cells were washed twice with cold PBS, then scraped in cold PBS and pelleted at 3,000 rpms. The pellet was then resuspended in 1% SDS sonication buffer (50mM Tris-HCl pH 8.0, 10mM EDTA) and sonicated using a Fisher Scientific 550 Sonic Dismembrator. Using a cycle setting of 7,

lysates were sonicated for 15 sec followed by a 30 sec rest; 2 sets of 6 pulses were performed to acquire sheared DNA between 200-1000bp. Lysates were then cleared at 14,000 rpms for 10 min at 4°C; 500ug of chromatin was used for each IP. Antibodies used for ChIP: anti-RXR (ΔN 197, Santa Cruz Biotechnology) and Rabbit IgG (sc2027, Santa Cruz Biotechnology). Primers for ChIP analysis were designed according to LXREs identified by ChipSeq[25].

**Isolation of endogenous LXR with GW3965-affinity beads—**Female mice fed HF/HC/BS diet were fed HF/HC/BS diet for 6 weeks, and infected with CMV-Ubc adenovirus (Vector Biolabs) during the last week. Mice were given an oral gavage of the proteasomal inhibitor ixazomib (20 mg $kg^{-1}$ in 40% 2-hydroxypropyl-β-cyclodextrin, Selleckchem) and then fasted for 6 h before sacrifice. GW3965 HCl (Selleckchem) was coupled to M-270 amine Dynabeads (Invitrogen) in a nitrogen-purged reaction containing N-(3-Dimethylaminopropyl)-*N′*-ethylcarbodiimide, 4-(Dimethylamino)pyridine, and tributylamine in dimethylformamide (Sigma). Replacing the carboxylic acid in GW3965 with an amide in the coupling reaction allows the synthetic LXR agonist to retain its ligand binding domain recruitment activity[38]. Livers from HF/HC/BS diet-fed mice were sonicated in HEPES lysis buffer (50 mM HEPES, 150 mM NaCl, 1% NP-40, 10% glycerol, 5 mM EDTA, pH 7,4) supplemented with 10 mM N-ethylmaleimide, 10 mM iodoacetamide (Sigma), 25 μM PR-619 (Calbiochem), 5 μM MG-132 (Selleckchem), TUBE-2 (LifeSensors) and Halt Protease Inhibitor Cocktail (Thermo Scientific). Liver lysates were incubated with GW3965-beads at 37°C for 2 h.

**LXRα protein turnover—**FLAG-Myc-LXRα-transfected primary hepatocytes were cultured in methionine-free media for 1 h, and then protein synthesis was labelled with 400 μM L-homopropargylglycine (HPG) for 30 min. The labelled primary hepatocytes were washed and then cultured in 20 mM L-methionine-enriched media with/without bortezomib for the duration of the chase. FLAG-Myc-LXRα was immunoprecipitated with anti-FLAG (clone M2)-conjugated magnetic beads (Sigma-Aldrich) and HPG-labelled proteins were conjugated to tetramethylrhodamine azide by click chemistry (Molecular Probes) prior to separation by SDS-PAGE for visualization.

**Statistical Analysis—**All data are represented as mean ± SEM and unless otherwise, were analyzed using the two-tailed Student t-test or two-way ANOVA with Bonferroni post hoc analysis where appropriate. In experiments where $n \geq 8$ for all genotypes, the D'Agostino-Pearson omnibus test for normality and Bartlett's test for variance were used to ensure the assumptions of the statistical tests were met. All tests were performed with Prism 4 (Graphpad) and $p < 0.05$ was considered statistically significant. Values/animals were excluded if it was detected as a significant ($p<0.05$) outlier based on the two-sided Grubbs' test.

## Extended Data

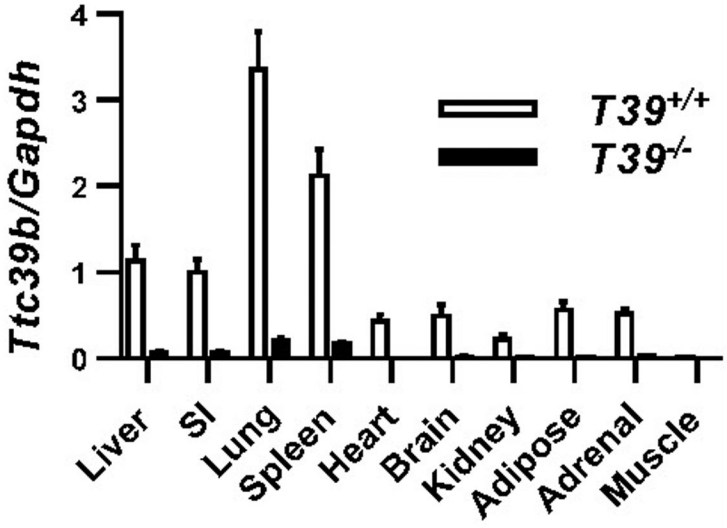


**ED Fig 1. Organ distribution of T39 mRNA expression**

*T39* mRNA levels were assessed in chow-fed male WT and whole body T39 knockout mice, small intestine is abbreviated as "SI," n=4 animals per genotype.

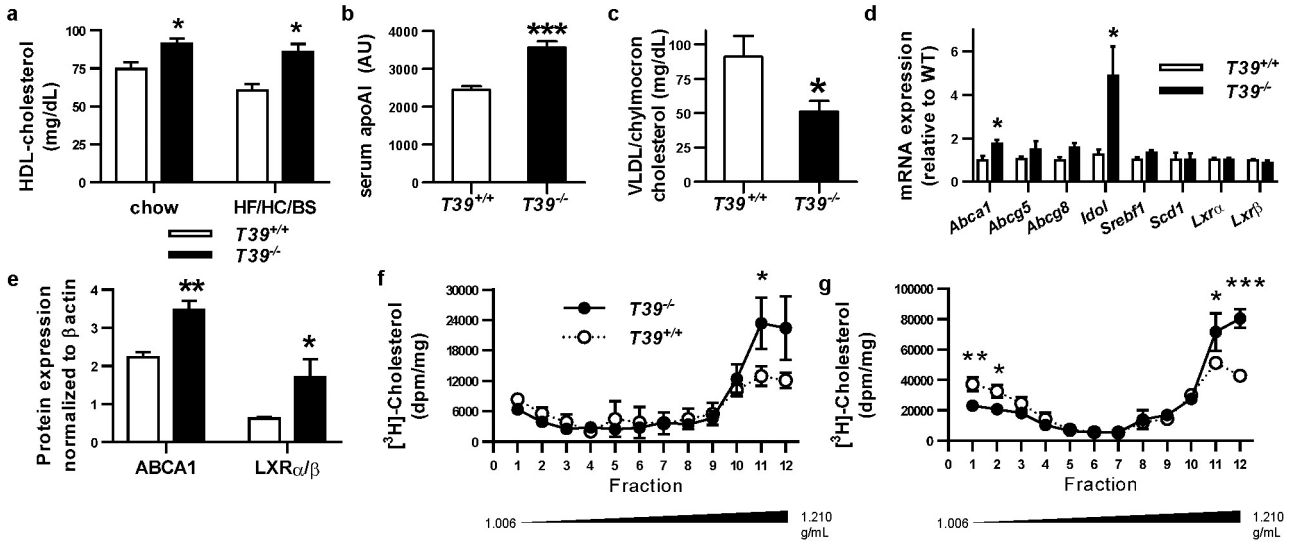


**ED Fig 2. Beneficial lipoprotein changes in T39-deficient mice fed HF/HC/BS diet**

(a) HDL-cholesterol of WT and whole body T39 knockout mice fed chow or HF/HC/BS diet for 4 weeks, n=4 per genotype for chow, 5 per genotype for HF/HC/BS diet. (b) Serum ApoAI as determined by SDS-PAGE and (c) Serum VLDL/chylomicron cholesterol of WT and whole body T39 knockout mice fed HF/HC/BS diet for 4 weeks, n=5 per genotype. (d) Enterocyte mRNA expression, n=5 per genotype. (e) Quantification of enterocyte protein expression normalized to βactin, n=4 per genotype. (f) Cholesterol secretion profiles of enterocytes collected from WT and whole body T39 knockout mice fed chow or (g)

HF/HC/BS diet. Enterocytes were incubated with taurocholate micelles containing [$^3$H]cholesterol for 2 h , and then secreted lipoproteins were separated by density ultracentrifugation. Lipoprotein fractions are shown with fraction 1 being the most buoyant and fraction 12 the most dense, n=3 per genotype, and replicated in 2 different experiments. For all panels, data is represented as mean ± SEM, *p<0.05, **p<0.01 and ***p<0.001 by two-tailed Student's *t*-test.

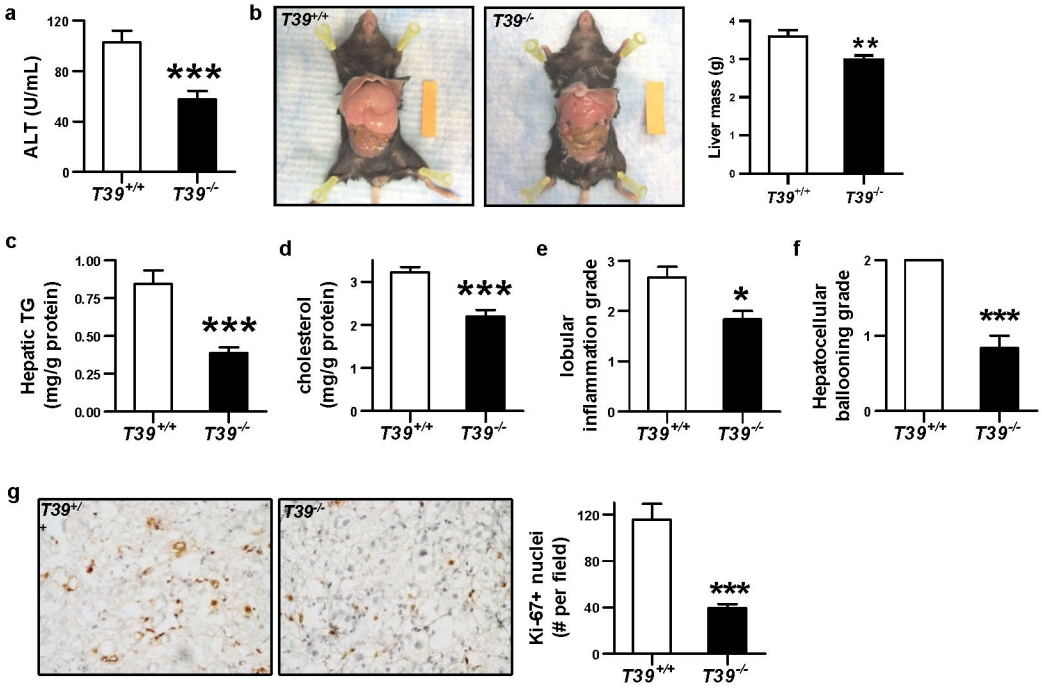


**ED Fig 3. Improved features of NASH in *T39*$^{-/-}$ mice fed HF/HC/BS diet**

WT and whole body T39 knockout mice were fed the HF/HC/BS diet for 18 weeks. (a) Serum ALT, (b) Liver size, (c) hepatic TG and (d) hepatic cholesterol content, n=15-19 per genotype. Grading of (e) inflammatory cell infiltration and (f) hepatocellular ballooning degeneration based on hematoxylin and eosin-stained sections, n=6 per genotype. (g) Ki-67 was immunohistochemically detected with diaminobenzidine (brown) in frozen liver sections with nuclei counterstained with hematoxylin (blue). Quantification of Ki-67-positive nuclei is shown on the right, mean of 5 fields, n=6 animals/genotype. Data is represented as mean ± SEM, ***p<0.001 by two-tailed t-test.

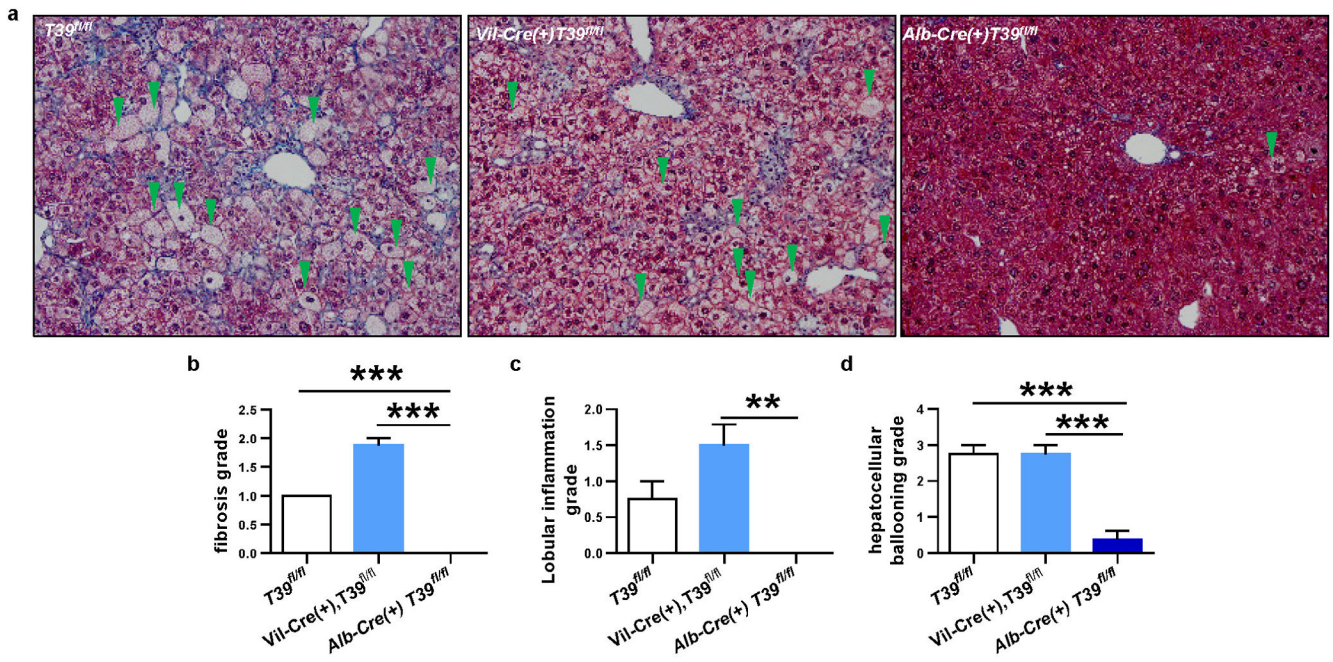


**ED Fig 4. Improvements in the histological features of NASH in liver-specific T39 knockout**

Enterocyte- and hepatocyte-specific T39 knockout and *T39*$^{fl/fl}$ control mice were fed HF/HC/BS diet for 21 weeks. (a) Representative Masson's trichrome stain of hepatic sections at 100× magnification, showing cytoplasm as red, collagen as blue, and nuclei as dark brown. Grading of (b) fibrosis severity, (c) inflammatory foci number and (d) extent of hepatocellular ballooning based on Masson's trichrome staining, n=4 per genotype. Data is represented as mean ± SEM, **p<0.01, ***p<0.001 by one-way ANOVA.

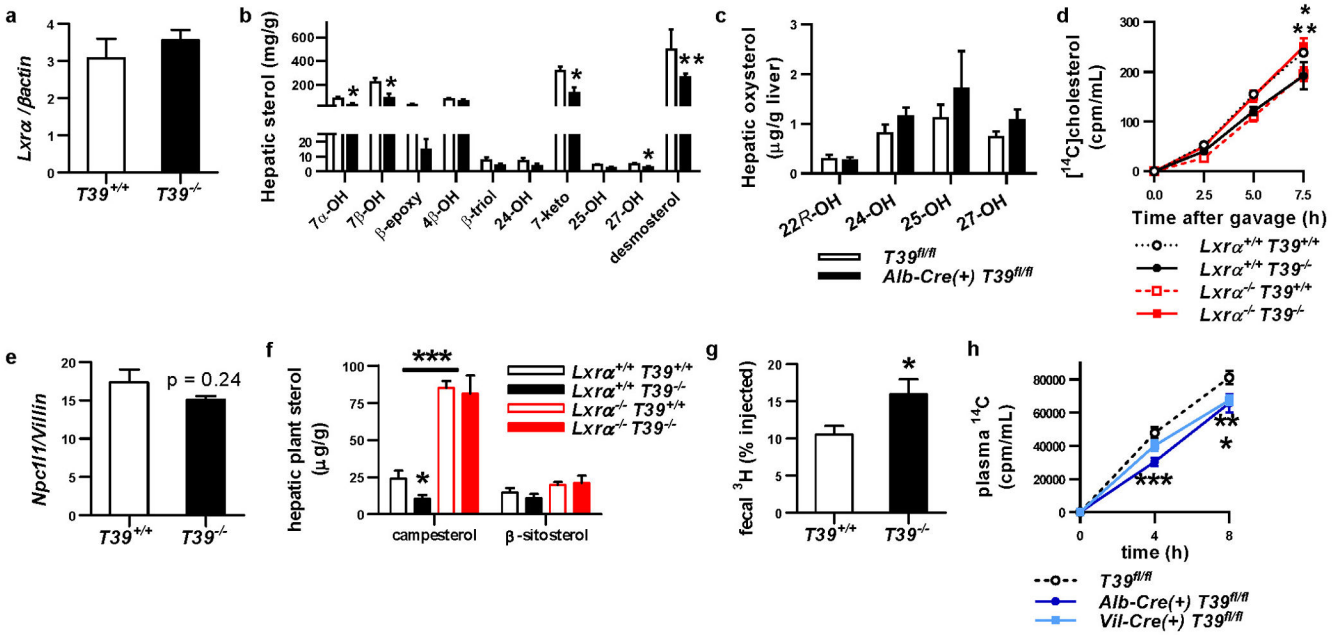

**ED Fig 5. Decreased dietary cholesterol absorption in T39-deficient mice fed HF/HC/BS diet**

(a) Hepatic *Lxrα* mRNA expression in mice fed HF/HC/BS diet for 5 weeks, n=4 per genotype. (b) Hepatic oxysterol content of WT and whole body T39 knockout mice fed HF/HC/BS diet for 18 weeks, n=5 WT and 4 $T39^{-/-}$. (c) Hepatic content of endogenous LXR ligands in control and liver-specific T39 knockout mice fed HF/HC/BS diet, n=7 per genotype. (d) Absorption of [$^{14}$C]cholesterol administered by gavage to WT and whole body T39 knockout with/without LXRα along with Poloxamer-407 injection to inhibit peripheral lipoprotein catabolism, n= 3 $Lxra^{+/+}T39^{+/+}$, 4 $Lxra^{+/+}T39^{-/-}$, 3 $Lxra^{-/-}T39^{+/+}$, and 5 $Lxra^{-/-}T39^{+/+}$. (e) Enterocyte *Npc1l1* mRNA expression in WT and whole body T39 knockout mice, n=5 per genotype. (f) Hepatic plant sterol content of WT, whole body T39 knockout, LXRα knockout, and LXRα T39 double knockout mice fed HF/HC/BS diet for 6 weeks, n= 4 $Lxra^{+/+}T39^{+/+}$, 4 $Lxra^{+/+}T39^{-/-}$, 4 $Lxra^{-/-}T39^{+/+}$, and 6 $Lxra^{-/-}T39^{+/+}$. (g) Reverse cholesterol transport of WT and whole body T39 knockout mice fed HF/HC/BS diet. $^{3}$H fecal excretion was measured over 3 days following an intravenous injection of [$^{3}$H]cholesteryl ester-labelled HDL, n=7 WT and 5 $T39^{-/-}$. (h) Absorption of [$^{14}$C]cholesterol administered by gavage to tissue-specific T39 knockout mice fed HF/HC/BS diet for 5 weeks and injected with Poloxamer-407, n=8 $T39^{fl/fl}$, 7 *Vil-Cre(+)*$T39^{fl/fl}$, and 9 *Alb-Cre(+)*$T39^{fl/fl}$. Data is represented as mean ± SEM, *p<0.05, **p<0.01, ***p<0.001 by two-tailed t-test or two-way ANOVA for absorption studies.

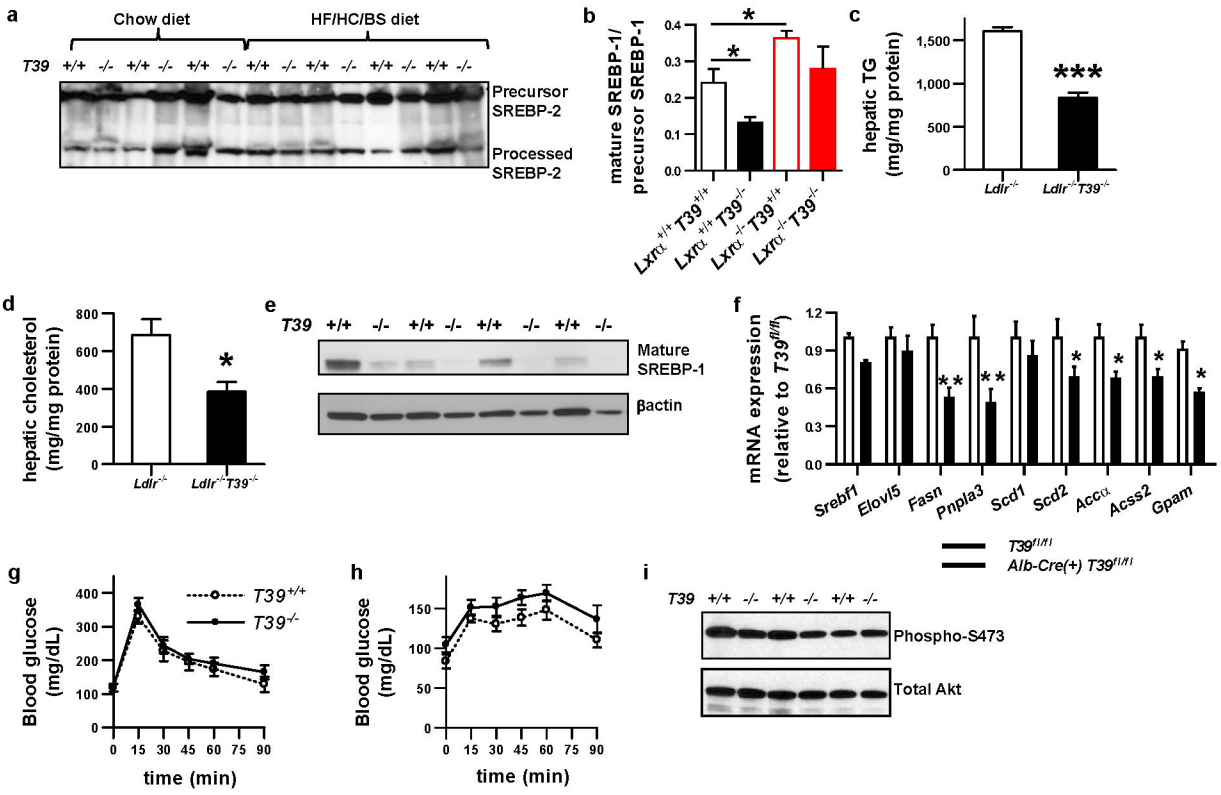


**ED Fig 6. Decreased SREBP-1 processing without altered hepatic insulin sensitivity in T39-deficient mice**

(a) Hepatic protein expression of precursor SREBP-2 (upper band) and processed SREBP-2 (lower band) of WT and whole body T39 knockout mice fed HF/HC/BS diet for 5 weeks. (b) SREBP-1 processing ratio in WT and whole body T39 knockout mice with/without LXRα fed HF/HC/BS diet for 6 weeks as based on quantification of an anti-SREBP-1 immunoblot, n=4 per genotype. (c) Hepatic TG and (d) cholesterol content of WT and whole body T39 knockout mice lacking LDLR fed WTD for 20 weeks, n=5 per genotype. (e) Protein expression of the nuclear form of SREBP-1 (top) and βactin loading control (bottom) of WTD-fed WT and whole body T39 knockout mice lacking LDLR fed WTD for 20 weeks. (f) Hepatic gene expression in liver-specific T39 knockout and control animals fed HF/HC/BS diet for 18 weeks, following a fasting/refeeding protocol, n=13 *T39*$^{fl/fl}$ and 7 *Alb-Cre(+)T39*$^{fl/fl}$. (g) Intraperitoneal glucose tolerance of WT and whole body T39 knockout mice fed HF/HC/BS diet after a 6 h fast, n=8 WT and 12 *T39*$^{-/-}$. (h) Pyruvate tolerance of WT and whole body T39 knockout mice fed HF/HC/BS diet after an overnight fast, n=5 WT and 7 *T39*$^{-/-}$. (i) Hepatic Akt phosphorylation 5 min after portal vein delivery of insulin in WT or whole body T39 knockout mice fed HF/HC/BS diet. Data is represented as mean ± SEM, *p<0.05, ** p<0.01, ***p<0.001 by two-tailed Student's *t*-test. See Supplementary Fig 1 for gel source data.

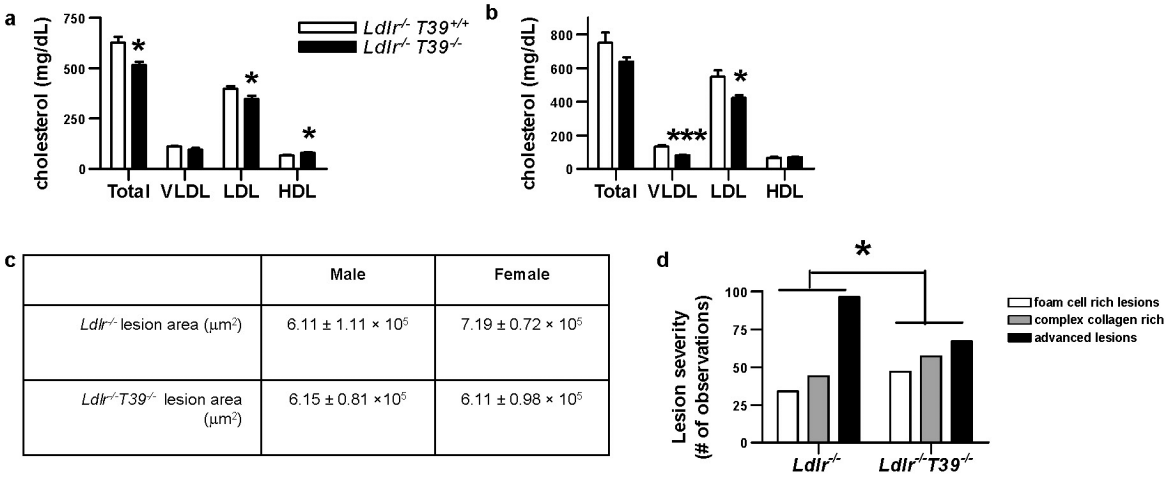


| c | Male | Female |
|---|---|---|
| *Ldlr*$^{-/-}$ lesion area (μm$^2$) | 6.11 ± 1.11 × 10$^5$ | 7.19 ± 0.72 × 10$^5$ |
| *Ldlr*$^{-/-}$*T39*$^{-/-}$ lesion area (μm$^2$) | 6.15 ± 0.81 ×10$^5$ | 6.11 ± 0.98 × 10$^5$ |

**ED Fig 7. Improved lipoprotein profile and less advanced atherosclerotic lesions in *Ldlr*$^{-/-}$*T39*$^{-/-}$ mice**

Mice on the *Ldlr*-/- background were fed WTD for 20 weeks. Serum lipoprotein cholesterol levels in (a) male and (b) female mice after 2 week on WTD, n=5 per genotype per gender. (c) Proximal aorta atherosclerotic lesion area after 20 weeks on WTD, n=5 animals per genotype per gender. Data is represented as mean ± SEM, *p<0.05, ***p<0.001 by two-tailed Student's *t*-test. (d) Lesion severity as graded by a blinded observer on 6 sections per animal, n=5 per genotype per gender. Lesion severity is expressed as number of observations of each complexity category and the difference in the categorical distribution of lesions between the two groups are indicated, *p<0.05 based on $\chi^2$-test.

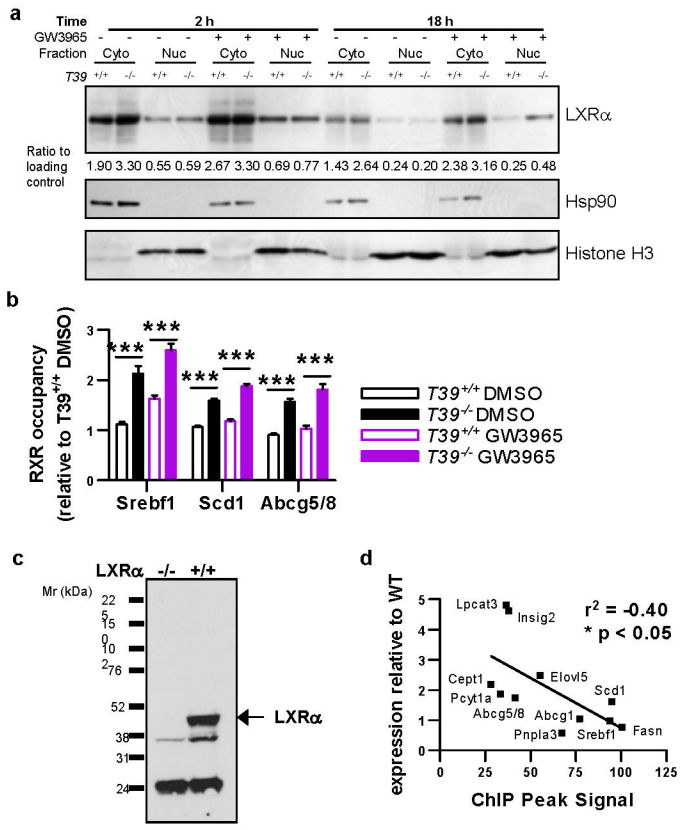


**ED Fig 8. Increased LXRα protein in T39-deficient hepatocytes has implications for LXR target gene expression**

(a) Immunoblots of endogenous LXRα in the nuclear (Nuc) and cytoplasmic (Cyto) fractions with an anti-LXRα antibody (top) 2 and 18 h after hepatocyte isolation and treatment with 2 μM GW3965. Histone H3 (bottom) and Hsp90 (middle) are shown as loading controls for nuclei and cytoplasm, respectively. Normalization of LXRα signal to the appropriate loading control is shown below the LXRα blot. The immunoblot is representative of 3 different sets. (b) RXR occupancy over LXREs of WT and T39 knockout primary hepatocytes treated with GW3965, n=4 WT and 5 *T39*$^{-/-}$. (c) Immunoblot showing validation of immobilized GW3965-mediated pulldown of endogenous LXRα from liver lysates. (d) Relationship between magnitude of LXR target gene induction in T39 knockout mice and LXR affinity to active regulatory elements in the liver. See Supplementary Fig 1 for gel source data.

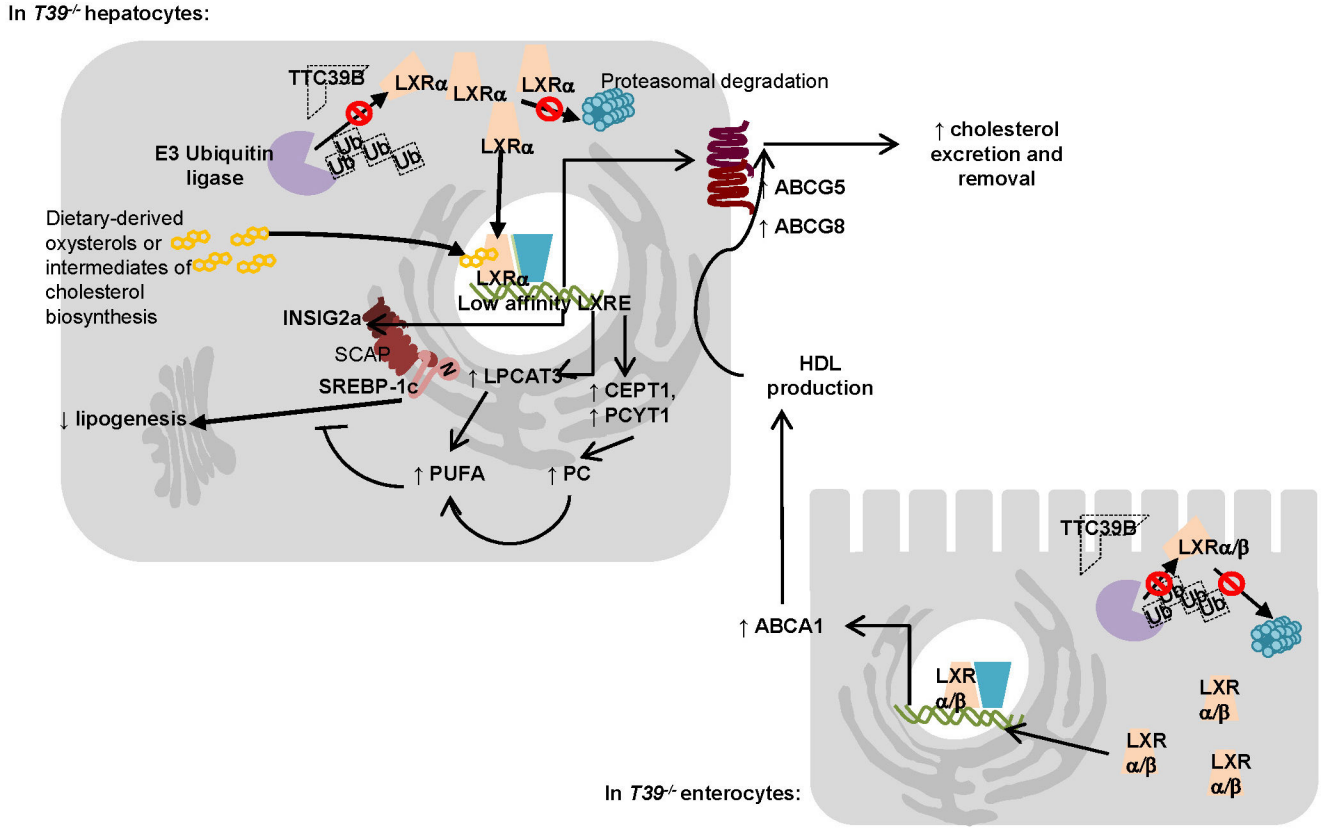


**ED Fig 9. LXR protein preservation in T39-deficient gastrointestinal tissues raises HDL and protect from steatohepatitis**

In the absence of T39, LXR assembly into a multiprotein complex that conjugates it to ubiquitin moieties does not occur, and LXR is spared from proteasomal degradation. In enterocytes, the increase in LXRα/β protein upregulates *Abca1* mRNA expression and promotes HDL production. In the liver, LXRα protein increase leads to the induction of *Abcg5/8*, which decreases dietary cholesterol uptake and increases cholesterol excretion, leading to cholesterol lowering. LXRα-mediated *Insig2a* prevents SREBP-1 processing in the fasted state, while *Pcyt1a*, and *Cept1* induction increases microsomal membrane phosphatidylcholine content that continues to inhibit SREBP-1 processing in postprandial state. LPCAT3 induction resulted in increased incorporation of PUFA into phospholipid species which also contributed to the decrease in SREBP-1 processing. The decrease in nuclear SREBP-1 prevents the induction of lipogenic genes such as *Fasn*. Therefore, unlike the gene expression profile that arises from potent synthetic ligands, increasing endogenous LXRα protein levels preferentially upregulates cholesterol removal pathways while inhibiting lipogenesis.

## Supplementary Material

Refer to Web version on PubMed Central for supplementary material.

## Acknowledgments

We would like to express our gratitude to F. Matsuura for support, A. Morishita for advice on liver histology, M. Sakurai and T. Yamashita for advice on immunoprecipitation experiments, W.R. Lagor for advice on the reverse cholesterol transport study, M. Ishibashi for advice on animal administration, J.W. Medley for consultation on the coupling reaction, and N. Wang for project discussions. D.J. Gorman and J. So provided technical support, and O. Xu provided technical services for the lipidomics analysis. This work was supported by grants from Manpei Suzuki Diabetes Foundation (M.K.), VIDI grant 91715350 from the Netherlands Organization of Sciences (M.W.), Rosalind Franklin Fellowship from the University Medical Center Groningen (M.W.), JSPS KAKENHI Grant #15K160203 (I.I.), and the Fondation Leducq (A.R.T.). This work was supported by grants from the National Institutes of Health (T32 training program HL007343, M.M.M; HL871233 and HL11983, A.R.T.; HL101864 and HL111398, D.J.R; DK46900, M.M.H.).

## References

1. Musso G, Gambino R, Cassader M, Pagano G. A meta-analysis of randomized trials for the treatment of nonalcoholic fatty liver disease. Hepatology. 2010; 52:79–104. [PubMed: 20578268]
2. Teslovich TM, et al. Biological, clinical and population relevance of 95 loci for blood lipids. Nature. 2010; 466:707–713. [PubMed: 20686565]
3. Willer CJ, et al. Discovery and refinement of loci associated with lipid levels. Nat Genet. 2013
4. McNeish J, et al. High density lipoprotein deficiency and foam cell accumulation in mice with targeted disruption of ATP-binding cassette transporter-1. Proceedings of the National Academy of Sciences of the United States of America. 2000; 97:4245–4250. [PubMed: 10760292]
5. Brunham LR, et al. Intestinal ABCA1 directly contributes to HDL biogenesis in vivo. The Journal of clinical investigation. 2006; 116:1052–1062. DOI: 10.1172/JCI27352 [PubMed: 16543947]
6. Wu AL, Windmueller HG. Relative contributions by liver and intestine to individual plasma apolipoproteins in the rat. The Journal of biological chemistry. 1979; 254:7316–7322. [PubMed: 457683]
7. Costet P, Luo Y, Wang N, Tall AR. Sterol-dependent transactivation of the ABC1 promoter by the liver X receptor/retinoid X receptor. J Biol Chem. 2000; 275:28240–28245. [PubMed: 10858438]
8. Zelcer N, Hong C, Boyadjian R, Tontonoz P. LXR regulates cholesterol uptake through Idol-dependent ubiquitination of the LDL receptor. Science. 2009; 325:100–104. [PubMed: 19520913]
9. Matsuzawa N, et al. Lipid-induced oxidative stress causes steatohepatitis in mice fed an atherogenic diet. Hepatology. 2007; 46:1392–1403. [PubMed: 17929294]
10. Rong X, et al. LXRs Regulate ER Stress and Inflammation through Dynamic Modulation of Membrane Phospholipid Composition. Cell metabolism. 2013; 18:685–697. [PubMed: 24206663]
11. Bensinger SJ, et al. LXR signaling couples sterol metabolism to proliferation in the acquired immune response. Cell. 2008; 134:97–111. [PubMed: 18614014]
12. Lo Sasso G, et al. Intestinal specific LXR activation stimulates reverse cholesterol transport and protects from atherosclerosis. Cell Metab. 2010; 12:187–193. [PubMed: 20674863]
13. Zhang Y, et al. Liver LXRalpha expression is crucial for whole body cholesterol homeostasis and reverse cholesterol transport in mice. J Clin Invest. 2012; 122:1688–1699. [PubMed: 22484817]
14. Yu L, et al. Overexpression of ABCG5 and ABCG8 promotes biliary cholesterol secretion and reduces fractional absorption of dietary cholesterol. J Clin Invest. 2002; 110:671–680. [PubMed: 12208868]
15. Repa JJ, et al. Regulation of mouse sterol regulatory element-binding protein-1c gene (SREBP-1c) by oxysterol receptors, LXRalpha and LXRbeta. Genes Dev. 2000; 14:2819–2830. [PubMed: 11090130]
16. Hegarty BD, et al. Distinct roles of insulin and liver X receptor in the induction and cleavage of sterol regulatory element-binding protein-1c. Proc Natl Acad Sci U S A. 2005; 102:791–796. [PubMed: 15637161]
17. Huang Y, et al. A feed-forward loop amplifies nutritional regulation of PNPLA3. Proc Natl Acad Sci U S A. 2010; 107:7892–7897. [PubMed: 20385813]
18. Romeo S, et al. Genetic variation in PNPLA3 confers susceptibility to nonalcoholic fatty liver disease. Nat Genet. 2008; 40:1461–1465. [PubMed: 18820647]

19. Vatner DF, et al. Insulin-independent regulation of hepatic triglyceride synthesis by fatty acids. Proc Natl Acad Sci U S A. 2015; 112:1143–1148. [PubMed: 25564660]
20. Walker AK, et al. A conserved SREBP-1/phosphatidylcholine feedback circuit regulates lipogenesis in metazoans. Cell. 2011; 147:840–852. [PubMed: 22035958]
21. Hishikawa D, et al. Discovery of a lysophospholipid acyltransferase family essential for membrane asymmetry and diversity. Proc Natl Acad Sci U S A. 2008; 105:2830–2835. [PubMed: 18287005]
22. Rong X, et al. Lpcat3-dependent production of arachidonoyl phospholipids is a key determinant of triglyceride secretion. Elife. 2015; 4
23. Hannah VC, Ou J, Luong A, Goldstein JL, Brown MS. Unsaturated fatty acids down-regulate srebp isoforms 1a and 1c by two mechanisms in HEK-293 cells. J Biol Chem. 2001; 276:4365–4372. [PubMed: 11085986]
24. Kammoun HL, et al. GRP78 expression inhibits insulin and ER stress-induced SREBP-1c activation and reduces hepatic steatosis in mice. J Clin Invest. 2009; 119:1201–1215. [PubMed: 19363290]
25. Boergesen M, et al. Genome-wide profiling of liver X receptor, retinoid X receptor, and peroxisome proliferator-activated receptor alpha in mouse liver reveals extensive sharing of binding sites. Mol Cell Biol. 2012; 32:852–867. [PubMed: 22158963]
26. Lehrke M, et al. Diet-dependent cardiovascular lipid metabolism controlled by hepatic LXRalpha. Cell Metab. 2005; 1:297–308. [PubMed: 16054077]
27. Perreault N, Beaulieu JF. Primary cultures of fully differentiated and pure human intestinal epithelial cells. Exp Cell Res. 1998; 245:34–42. [PubMed: 9828099]
28. Anwar K, Iqbal J, Hussain MM. Mechanisms involved in vitamin E transport by primary enterocytes and in vivo absorption. J Lipid Res. 2007; 48:2028–2038. [PubMed: 17582142]
29. Iqbal J, Anwar K, Hussain MM. Multiple, independently regulated pathways of cholesterol transport across the intestinal epithelial cells. J Biol Chem. 2003; 278:31610–31620. [PubMed: 12775725]
30. Kleiner DE, et al. Design and validation of a histological scoring system for nonalcoholic fatty liver disease. Hepatology. 2005; 41:1313–1321. [PubMed: 15915461]
31. Tomoyori H, et al. Phytosterol oxidation products are absorbed in the intestinal lymphatics in rats but do not accelerate atherosclerosis in apolipoprotein E-deficient mice. The Journal of nutrition. 2004; 134:1690–1696. [PubMed: 15226455]
32. Bligh EG, Dyer WJ. A rapid method of total lipid extraction and purification. Canadian journal of biochemistry and physiology. 1959; 37:911–917. DOI: 10.1139/o59-099 [PubMed: 13671378]
33. Dzeletovic S, Breuer O, Lund E, Diczfalusy U. Determination of cholesterol oxidation products in human plasma by isotope dilution-mass spectrometry. Analytical biochemistry. 1995; 225:73–80. DOI: 10.1006/abio.1995.1110 [PubMed: 7778789]
34. Spady DK, Dietschy JM. Sterol synthesis in vivo in 18 tissues of the squirrel monkey, guinea pig, rabbit, hamster, and rat. J Lipid Res. 1983; 24:303–315. [PubMed: 6842086]
35. Chan RB, et al. Comparative lipidomic analysis of mouse and human brain with Alzheimer disease. The Journal of biological chemistry. 2012; 287:2678–2688. DOI: 10.1074/jbc.M111.274142 [PubMed: 22134919]
36. Stary HC, et al. A definition of advanced types of atherosclerotic lesions and a histological classification of atherosclerosis. A report from the Committee on Vascular Lesions of the Council on Arteriosclerosis, American Heart Association. Circulation. 1995; 92:1355–1374. [PubMed: 7648691]
37. Gijbels MJ, et al. Progression and regression of atherosclerosis in APOE3-Leiden transgenic mice: an immunohistochemical study. Atherosclerosis. 1999; 143:15–25. [PubMed: 10208477]
38. Collins JL, et al. Identification of a nonsteroidal liver X receptor agonist through parallel array synthesis of tertiary amines. Journal of medicinal chemistry. 2002; 45:1963–1966. [PubMed: 11985463]

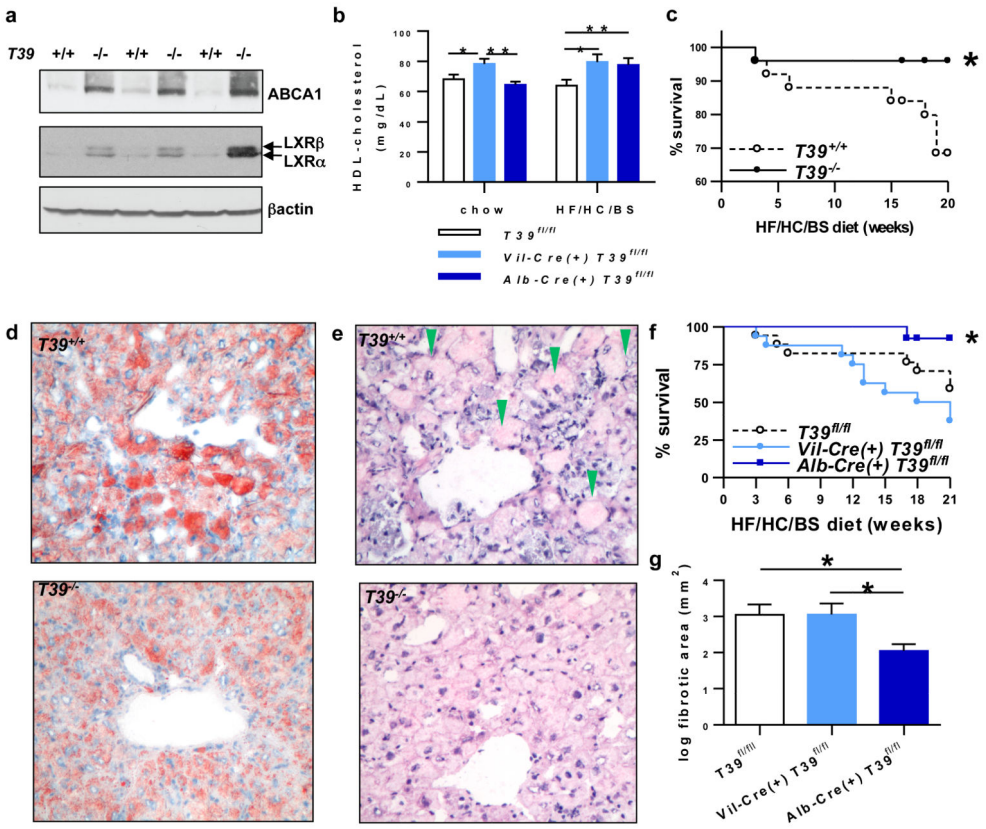


**Figure 1. Increased HDL-cholesterol and protection from steatohepatitis in T39-deficient mice**

(a) Enterocyte protein expression of ABCA1 (top), both LXR isoforms (middle), and βactin (bottom). (b) HDL-cholesterol of tissue-specific T39 knockout mice fed chow or HF/HC/BS diet for 2 weeks. (c) Mortality of WT and whole body T39 knockout mice fed the HF/HC/BS diet, *p<0.05 based on log rank test of the Kaplan-Meier curve, n=25 per genotype. (d) Representative Oil Red O and (e) hematoxylin and eosin stains of hepatic sections from female mice fed HF/HC/BS diet for 18 weeks. (f) Mortality of tissue-specific T39 knockout on the HF/HC/BS diet. For b and f, n=17 *T39*$^{fl/fl}$, 16 *Vil-Cre(+)T39*$^{fl/fl}$, and 13 *Alb-Cre(+)T39*$^{fl/fl}$, *p<0.05 based on log rank test of the Kaplan-Meier curve, n=13-17 per genotype. (g) Hepatic fibrotic area based on Masson's trichrome staining, n=8 per genotype. Data is represented as mean ± SEM, *p<0.05 and **p<0.01 by one-way ANOVA. See Supplementary Fig 1 for gel source data.

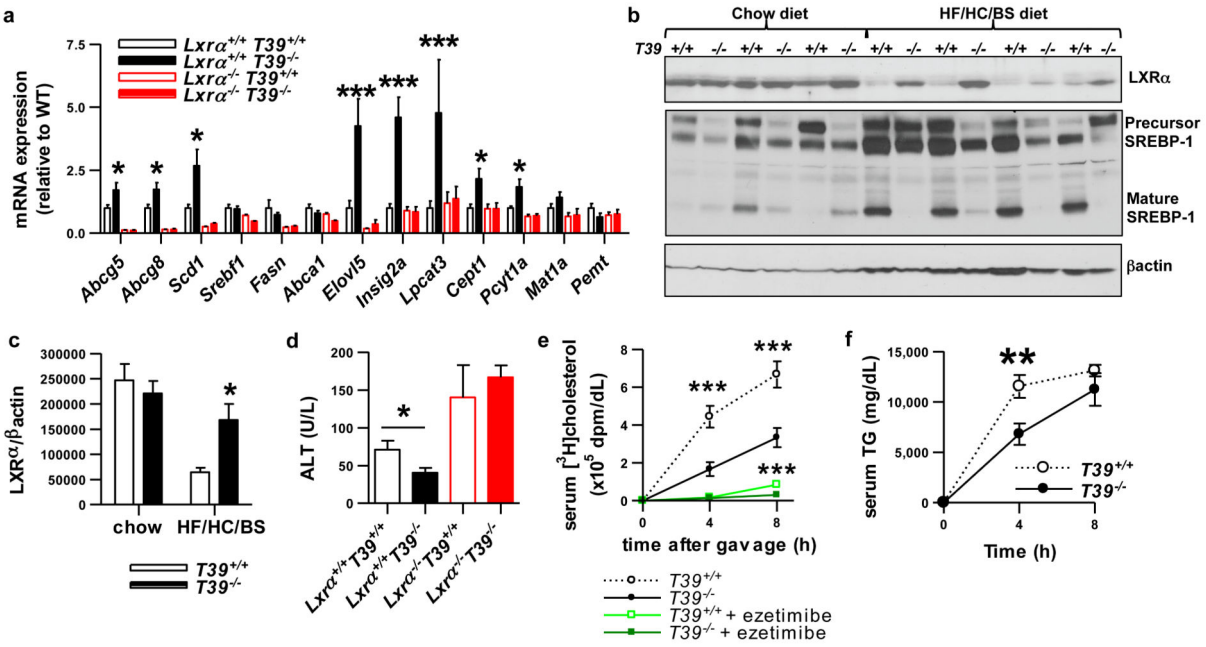


**Figure 2. Posttranscriptional LXR activation and decreased dietary cholesterol absorption in T39-deficient mice**

(a) Hepatic gene expression in fasted WT and whole body T39 knockout mice with/without LXRα fed HF/HC/BS diet for 6 weeks, ***p<0.001 by two-way ANOVA. (b) Hepatic protein expression of WT or whole body T39 knockout mice fed HF/HC/BS diet for 5 weeks, showing LXRα (top), both the microsomal and nuclear forms of SREBP-1 (middle), and βactin (bottom). (c) Quantification of LXRα protein, n=4 per genotype per diet. (d) Serum ALT levels of WT and whole body T39 knockout mice with/without LXRα fed HF/HC/BS diet for 2 weeks. For a and c, n= 7 *Lxrα*$^{+/+}$*T39*$^{+/+}$, 11 *Lxrα*$^{+/+}$*T39*$^{-/-}$, 8 *Lxrα*$^{-/-}$*T39*$^{+/+}$, and 4 *Lxrα*$^{-/-}$*T39*$^{+/+}$. (e) Short term dietary cholesterol absorption in WT and whole body T39 knockout mice fed HF/HC/BS diet for 4 weeks, with/without ezetimibe treatment, n=5 per genotype, ***p<0.001 by two-way ANOVA. (f) Postprandial TG secretion in WT and whole body T39 knockout mice, n=5 per genotype, **p<0.01 by two-way ANOVA. Data is represented as mean ± SEM, *p<0.05 and **p<0.01 by two-tailed t-test. See Supplementary Fig 1 for gel source data.

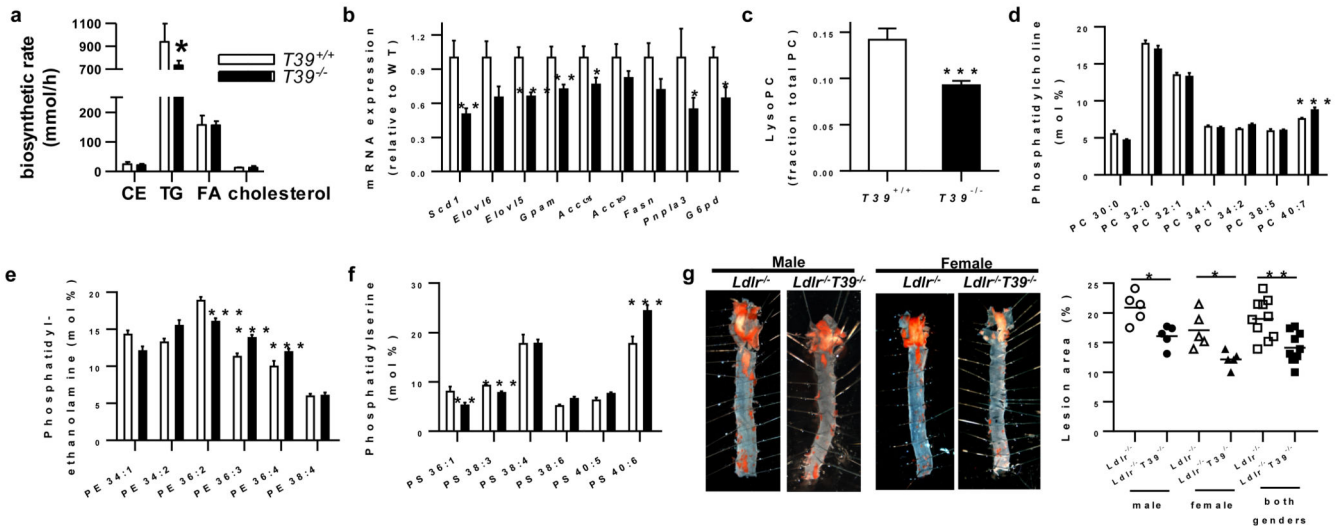


**Figure 3. Changes in phosphatidylcholine metabolism decreases lipogenesis along with reduced atherosclerosis**

(a) Hepatic lipid biosynthetic rate in WT or whole body T39 knockout mice fed WTD for 16 weeks, n=6 WT and 8 *T39*$^{-/-}$, **p<0.01 by two-ANOVA. (b) Hepatic lipogenic gene expression in fasted-refed mice fed WTD for 16 weeks, n=7 WT and 13 *T39*$^{-/-}$. (c) Lysophosphatidylcholine:phosphgatidylcholine ratio and the fatty acid composition of (d) phosphatidylcholine, (e) phosphatidylethanolamine and (f) phosphatidylserine in microsomes of livers from mice fed HF/HC/BS diet for 6 weeks, n=7 WT and 10 *T39*$^{-/-}$. (g) Atherosclerotic lesions of WT and whole body T39 knockout mice lacking LDLR fed WTD for 20 weeks, n=5 per genotype per gender. Data is represented as mean ± SEM, *p<0.05, **p<0.01, ***p<0.001 by two-tailed t-test. See Supplementary Fig 1 for gel source data.

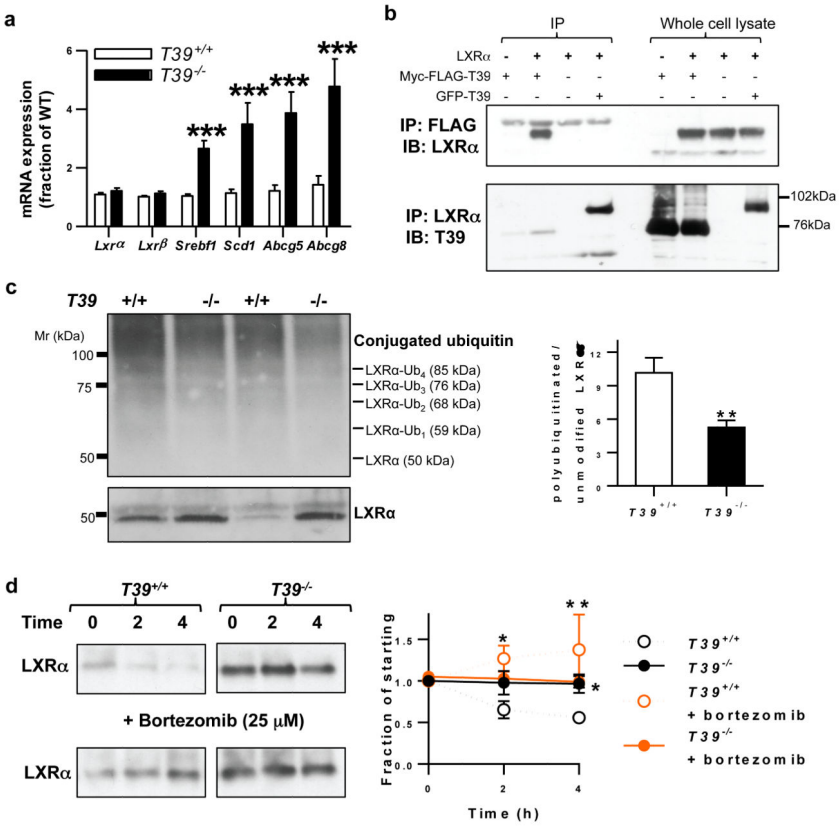


**Figure 4. T39 deficiency stabilizes LXRα in hepatocytes**

(a) Primary WT and T39 knockout hepatocyte mRNA expression, n=4 per genotype. (b) A protein complex containing LXRα and T39 as demonstrated by T39 immunoprecipiation (top) and the converse LXRα immunoprecipitation (bottom) shown on the left, while whole cell lysates are shown on the right. (c) *In vivo* ubiquitination of endogenous LXRα in livers of WT or whole body T39 knockout mice fed HF/HC/BS diet for 6 weeks and treated with a proteasomal inhibitor, ubiquitination signal of GW3965-mediated pulldown (top), unmodified LXRα (bottom), and quantification of the polyubiquitinated LXRα:unmodified LXRα ratio (right), n=10 per genotype. (d) Myc-FLAG-LXRα turnover in WT or T39 knockout hepatocytes with quantification of LXRα shown on the right,*p<0.05 and **p<0.01 versus WT by two-way ANOVA. Data is represented as mean ± SEM, **p<0.01, ***p<0.001 by two-tailed t-test. See Supplementary Fig 1 for gel source data.